Performance of the GSN station WCI-IU, 1997-2009

A report in a series documenting the status of the Global Seismographic Network

Göran Ekström and Meredith Nettles

Waveform Quality Center
Lamont-Doherty Earth Observatory of Columbia University, New York

1   Station performance report: WCI

This report summarizes a number of observations that are relevant for assessing the past and current quality of the data recorded at one of the stations of the Global Seismographic Network. The purpose of the report is, in part, to document specific problems observed with the data. Some of these problems are related to errors in the available descriptions of station parameters: orientation of the sensors, response functions, polarities. In principle, such errors in the station metadata can be corrected by providing updated station parameters. In practice, this may be difficult in some cases due to lack of knowledge of, or inability to determine, the correct parameters. Other problems are caused by the malfunctioning of some instrument component. Regardless of the cause, it is necessary to document and publicize the lack of accurate and reliable station characteristics, especially when it is not obvious from simple inspection of the data that a problem exists. It is also of value to document the characteristics of stations performing well, both to establish their high quality and to help identify installation and operation procedures that should be emulated at other stations.

1.1   Station WCI

The station WCI (Wyandotte Cave) is located 30 km west of Louisville in southern Indiana (Figure 1). The closest GSN station is WVT (Waverly, Tennessee), approximately 250 km to the southwest. The station CCM lies ∼350 km to the west.

WCI is part of the USGS (IU) component of the IRIS/USGS Global Seismographic Network. WCI is also part of the USGS Advanced National Seismic System and the USArray Reference Network.

1.2   The data

Digital seismic data from WCI are available from the IRIS DMC beginning in 1997. Here, we consider the STS-1 sensor, which is the only broadband sensor operating at the station. Data from WCI are considered in our standard CMT analysis (Dziewonski et al., 1981; Ekström et al., 2005), and waveform data, travel-time observations, and dispersion curves derived from WCI data have been used in the development of numerous global and regional tomographic models since the station was installed.

In the analyses described here, we have made use of data collected from the IRIS DMC. We requested and downloaded all long-period (LH) and very-long-period (VH) data available at the DMC from the start

of operation (1997) until August 2009. We used the currently available station metadata prepared by the Albuquerque Seismological Laboratory and available at the IRIS DMC (downloaded in December 2009). Few data were recorded by the station during 1999–2001. The station has operated with few data outages since 2003.

1.3 The metadata

The dataless SEED volume for WCI documents four response epochs for the STS-1 sensor. The STS-1 1 sps channels were initially called LHZ, LHN, LHE, without a location code. On 2002.340, the STS-1 channels were renamed with the location code 00. We refer to these channels as LHZ-00, LHN-00, and LHE-00. Epoch boundaries are given at 1997.198 (first STS-1 data), 1999.316, 2002.340, and 2008.263. The metadata indicate no changes in gain or frequency characteristics of the STS-1 during the period 1997–2009.

1.4 Scaling analysis

One method for assessing the quality of the data is the systematic comparison of recorded long-period waveforms with synthetic seismograms calculated for known seismic events. This analysis follows the steps described by Ekström et al. (2006). Seismic data for the LH and VH channels from the STS-1 sensor are collected. Corresponding synthetic waveforms for all earthquakes in the Global CMT catalog (Dziewonski et al., 1981; Ekström et al., 2005) with $M_W \geq 6.5$ are calculated. Correlation coefficients and optimal scaling factors between observed and synthetic waveforms are calculated for the three types of data used in the standard CMT analysis: body waves (B), with periods in the range 50–150 sec, mantle waves (M), with periods in the range 125–350 sec, and surface waves (S), with periods in the range 50–150 sec. Body- and mantle-wave results are discussed here. The scaling factor is only calculated for waveforms with a correlation of 0.75 or greater. The scaling factor is the number by which the synthetic seismogram should be multiplied to maximize the agreement with the observed seismogram. Annual median values of the scaling factors are calculated when four or more individual event scaling estimates are available for the year. Reversed components can be identified by their large negative correlations.

Figure 2 shows the results of our systematic comparison of WCI waveforms with synthetic seismograms. The diagram shows serious problems with the data on all components. While sufficient correlation between observed and synthetic waveform is obtained for many events on all three components, scaling factors deviate significantly from 1.0 for most measurements. In 1997, the annual median intermediate-period body-wave and long-period mantle-wave scaling factor are similar to each other for the horizontal components. During the remainder of the operational period, the body- and mantle-wave scaling factors deviate significantly from each other, and from 1.0. On the vertical component, the body- and mantle-wave scaling factors never agree; they deviate significantly from 1.0 throughout the station's operational history.

Temporal variations in the scaling factors are evident, with early loss of long-period (mantle-wave period band) gain, and subsequent loss of intermediate-period gain.

1.5 Noise analysis

A second method for investigating the overall performance of the sensors is to monitor background noise levels for all seismic channels, after conversion of the data to ground acceleration. We calculate hourly rms values of the time-domain seismic signal in narrow frequency bands, and convert the rms values to a power spectral density (PSD) at that frequency using Parseval's theorem. For each month, we then calculate the low-noise value at each frequency by determining the PSD amplitude not exceeded 10% of the time.

The PSD data provide much information about the station and the sensors. Figure 3 shows the monthly low-noise estimate for each LH channel at 72-s period since 1997. The first observation is that the station has suffered one long period of low data recovery, from late 1998 until early 2002. Since 2003, there have been no long data outages. Second, the apparent noise levels at 72 s period have been variable. Immediately after installation, vertical and E–W noise levels increased dramatically. From 2002–2007, noise levels were relatively constant. Since 2008, vertical and E–W noise levels have again increased.

The monthly low-noise estimates at 193-s period (Figure 4) follow similar trends to those at 72-s period. However, at 193-s period, it is clear that the station response is incorrect, as vertical noise levels from 2003–2008 remain consistently below Peterson's (1993) Low Noise Model. These unrealistic low noise values at long periods are consistent with the loss of long-period gain seen in Figure 2. Starting in 2008, noise levels on the vertical component increase dramatically.

1.6 Inter-sensor coherence

An additional method for assessing the quality and calibration of the recorded signals is to calculate inter-sensor coherence. This analysis is possible when more than one sensor is operated in the same location (e.g., Ekström and Nettles, WQC Report 2010:1). Because only one broadband sensor is operated at WCI, no inter-sensor coherence analysis is possible for this station.

1.7 Polarization analysis

The orientation of the horizontal components can be assessed empirically by comparing observed and synthetic waveforms, and finding the angle by which the horizontal components should be rotated in order to maximize the agreement. We follow the approach described by Ekström and Busby (2008) for such a comparison, using the observed and synthetic waveforms from Global CMT analysis.

We apply the method of Ekström and Busby (2008) to the same dataset used in the scaling analysis. Figure 5 shows the individual measurements for the period of operation for the different channels. Overall, the number of useful observations for the STS-1 sensor is small, a consequence of the large errors in the responses of the horizontal components. The median estimates for the entire period of operation are given in Table 1. In general, the median observations are consistent with the orientations provided in the metadata, but the scatter in the estimates is large.

Comp. 1	Comp. 2	First	Last	# Obs.	N	Az 1	Az 2	25%	Med.	75%
LHE	LHN	19970719	20021012	77	17	90	0	-6	-2	0
LHE-00	LHN-00	20030104	20090830	286	28	90	0	-5	1	6

Table 1: Statistics of sensor-rotation angles estimated in this study. Columns are the channel names, the dates of the first and last observations considered in making the estimate, the total number of observations, the number of observations of acceptable quality, the reported azimuths of sensitivity of the two channels, the median polarization-angle deviation from the reported orientation together with the range of the second (25%) and third (75%) quartiles of the observations.

1.8 Example seismograms

The anomalies described here agree with observations we have made in our routine analysis of waveforms for the determination of CMT earthquake parameters. When confronted with the seismograms for an individual earthquake, it is often difficult to assess whether a poor fit is due to incorrect source parameters,

inadequate modeling of wave propagation through an Earth model, or some problem with the recorded seismograms. Here, we have included some examples of data that illustrate the characteristics of the types of problems that we have encountered with data from the WCI station.

Figure 6 shows an example of three-component STS-1 mantle-wave data for an earthquake on December 22, 1997, a few months after instrument installation. The observed vertical waveform, dominated by fundamental-mode Rayleigh wave arrivals, is very poorly fit. The synthetic seismogram is a factor of four larger than the observed. The Rayleigh wave arrivals recorded on the horizontal components are fit adequately, corroborating the suggestion that the vertical misfit is due to an instrument response error. The scaling factors for the horizontal components are also small (∼0.8) which is suggestive, but, for a single event, not diagnostic of, a too-small long-period gain.

The top panel of Figure 7 shows a comparison of surface-wave seismograms and the corresponding synthetic waveforms for an event on August 23, 1998, approximately one year after initial station installation. The seismograms are fit reasonably well in the intermediate-period surface-wave band, with the exception of the vertical component. The bottom panel shows the long-period mantle waves for the same event. All components show a loss of long-period gain, with scaling factors smaller than 0.5 for both the vertical and E–W components.

The top panel of Figure 8 shows a comparison of surface-wave seismograms and the corresponding synthetic waveforms for an event on August 3, 2009. Gross amplitude and phase mismatch is seen for all three components. Bottom panel shows the long-period mantle waves. Only the N–S component shows a significant correlation between observed and synthetic waveforms, and a scaling factor larger than 0.3.

2 Summary and analysis

At the time of writing (February, 2010), the GSN station WCI is essentially broken. The relative and absolute calibrations are unknown, on all three components. The malfunction of the instrument is evident in comparisons between observed and synthetic waveforms (Figure 8), in scaling analysis (Figure 2), and in noise analysis (Figure 3 and Figure 4).

The STS-1 seismometers appear to have malfunctioned soon after installation in 1997. Figure 2 and Figure 6 suggest that the vertical component may never have generated well-calibrated data. Both the scaling analysis (Figure 2) and the noise analysis (Figure 3) suggest that the instrument deteriorated quickly during the year following installation. By August 1998 (Figure 7), the E–W component had lost half of its long-period gain.

The station generated little data from 1999–2002. No improvement in data quality is evident when continuous data flow from the station resumes in 2003. The response at shorter periods has deteriorated further during 2004–present (Figure 2). No well-calibrated broadband data have been recorded by this station since 1998.

We are no longer able to use data from WCI in CMT analysis, in any frequency band.

3 Conclusions and recommendations

This analysis shows that WCI may never have generated data of GSN quality. Errors in the response functions in the long-period band exceed 50% for all channels for most of the time of operation, a period of more than 10 years. The response errors are clearly time dependent, which makes it unlikely that any retroactive remedy for the observed problems will be possible.

The sensor problems described here are consistent with symptoms reported by the WQC in 2004. The problems should have been identified and investigated early on, and corrected. We speculate that the problem went unnoticed or undiagnosed because no routine calibrations are performed at GSN stations. The lack of systematic calibrations, and inspection of calibration results, makes it difficult to identify instrument problems. In addition, the lack of calibrations makes it nearly impossible to repair errors in instrument parameters once a problem has been identified. The symptoms of the STS-1 malfunction are similar to those observed at other stations (Ekström et al., 2006, Ekström and Nettles, WQC Report 2010:2); interpretation is complicated by the presence of multiple sensor problems.

Modern seismological analyses require well-calibrated instruments. Amplitude variations of 10% and smaller are interpreted as signals in modern studies that seek to map the attenuating properties of the Earth's interior (e.g., Dalton and Ekström, 2006). Phase anomalies of a few seconds at long periods are similarly interpreted in terms of Earth's elastic structure by numerous authors. Data from WCI have been used in such studies with the assumption that the station is meeting GSN design goals (IRIS, 1985; Lay et al., 2002) with respect to instrument stability. Clearly it does not, and its failure to do so should be documented. This is particularly important when, as for WCI, the data may at times appear visually to be correct, but actually are faulty.

It is urgent to restore WCI to a state where it generates GSN-quality data. This is particularly important because WCI is a station of the USGS Advanced National Seismic System and a station of the USArray Reference Network. Considering the design and performance goals of the Transportable Array, it seems prudent to consider the results reported here in the deployment plans for the Transportable Array. Colocation of a broadband Transportable Array instrument at the WCI site might be a good option.

4   References

Dalton, C. A., and G. Ekström, Global models of surface wave attenuation, *J. Geophys. Res.*, 111, B05317, 2006.

Dziewonski, A. M., T.-A. Chou, and J. H. Woodhouse, Determination of earthquake source parameters from waveform data for studies of global and regional seismicity, *J. Geophys. Res.*, 86, 2825–2853, 1981.

Ekström, G., A. M. Dziewonski, N. N. Maternovskaya, and M. Nettles, Global seismicity of 2003: Centroid-moment tensor solutions for 1087 earthquakes, *Phys. Earth Planet. Inter.*, 148, 327–351, 2005.

Ekström, G., C. A. Dalton, and M. Nettles, Observations of time-dependent errors in long-period gain at global seismic stations, *Seism. Res. Lett.*, 77, 12–22, 2006.

Ekström, G., and R. W. Busby, Measurements of seismometer orientation at USArray Transportable and Backbone stations, *Seism. Res. Lett.*, 79, 554-561, 2008.

Ekström, G., and M. Nettles, Performance of the GSN station CASY-IU, 1996–2009, Waveform Quality Center Report 2010:1, 2010.

Ekström, G., and M. Nettles, Performance of the GSN station KIP-IU, 1988–2009, Waveform Quality Center Report 2010:2, 2010.

IRIS, *The design goals for a new global seismographic network*, IRIS GSN committee report, 31 pages, 1985.

Lay, T., J. Berger, R. Buland, R. Butler, G. Ekström, B. Hutt, B. Romanowicz, *Global seismic network design goals update 2002*, IRIS GSN committee report, 2002.

Peterson, J., Observations and modeling of background seismic noise, *U. S. Geol. Surv. Open-file Rep. 93-322*, 1–45, 1993.
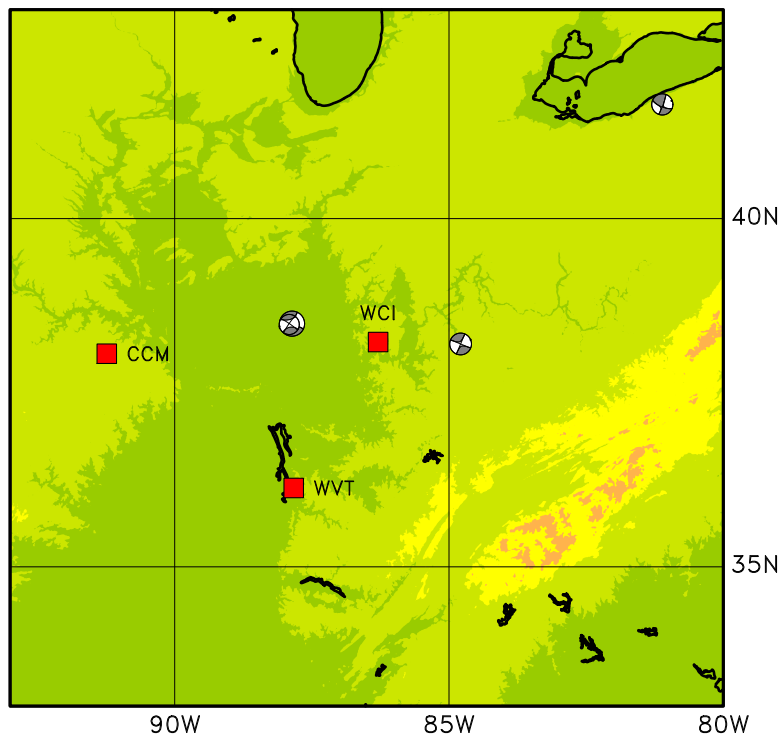
Figure 1: Map showing the location of WCI (red square in the center). Grey focal mechanisms show locations and moment tensors from the Global CMT catalog. The closest GSN station is WVT-IU, approximately 250 km to the southwest. The station CCM-IU is located to the west.
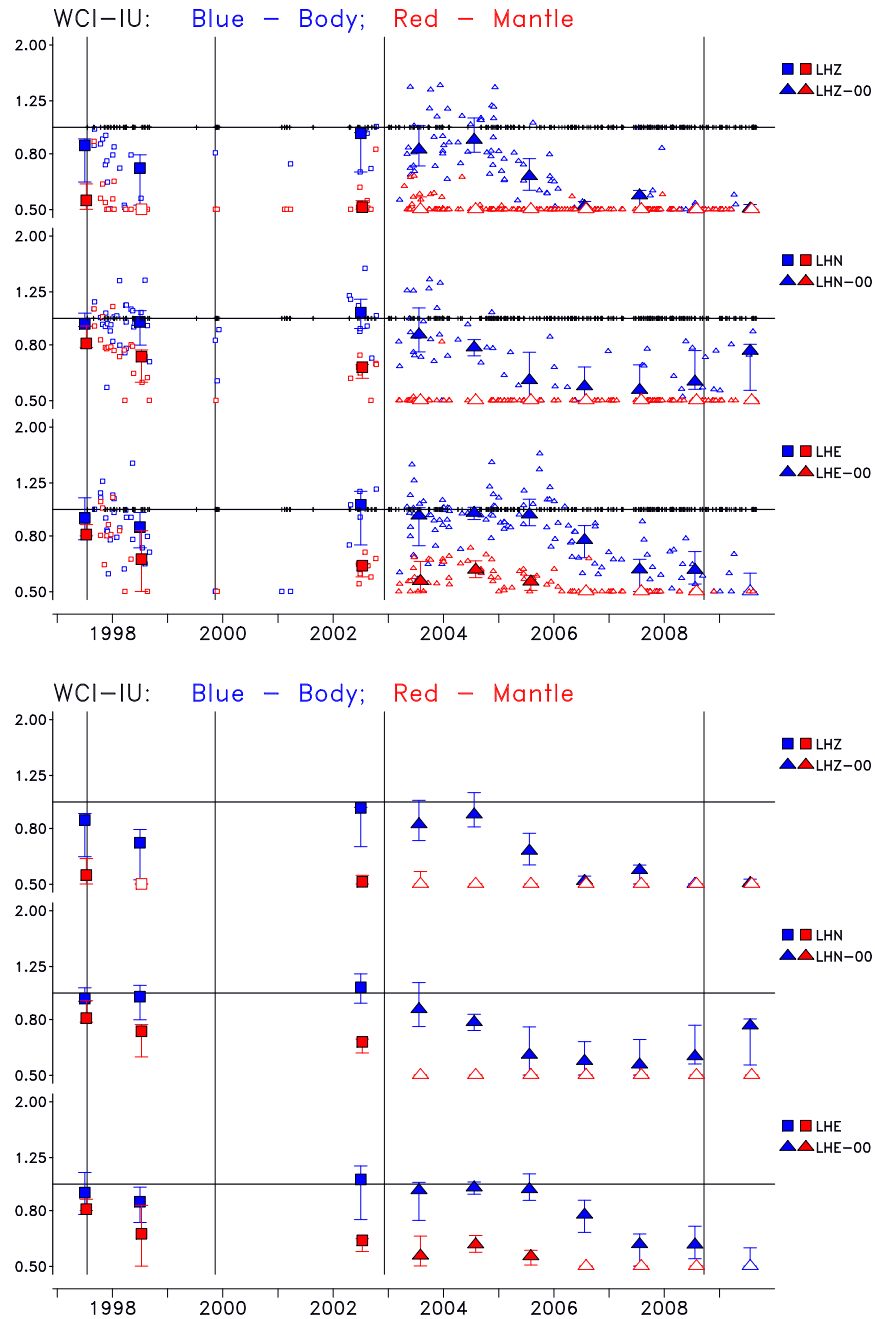
Figure 2: Scaling factors for the data channels at WCI. Small symbols in top panel show scaling factors for individual traces. Tick marks on the horizontal axes show times of observations for which the correlation was less than 0.75. Large symbols show the median scaling factor for each year, with the error bars corresponding to the range of the second and third quartiles of the scaling factors. The legend on the right identifies the symbol type with a specific channel. Open large symbols indicate that the annual scaling factor was smaller than 0.5. Thin vertical lines show the response epoch boundaries present in the metadata. Bottom panel shows only the annual median values.
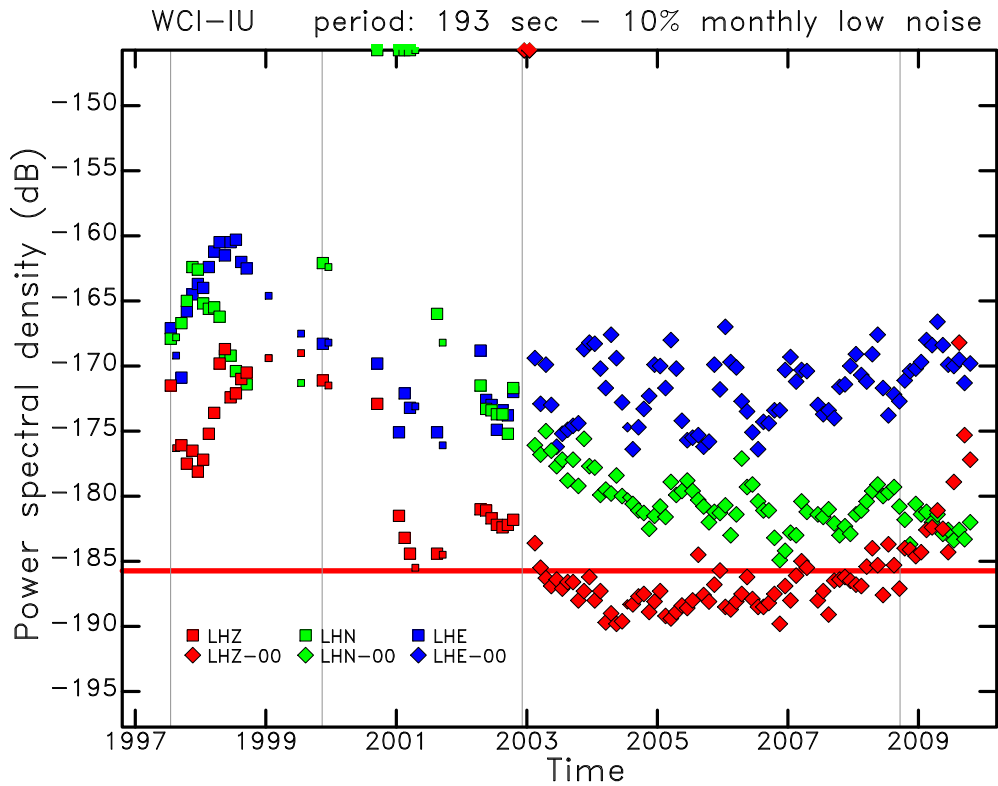
7
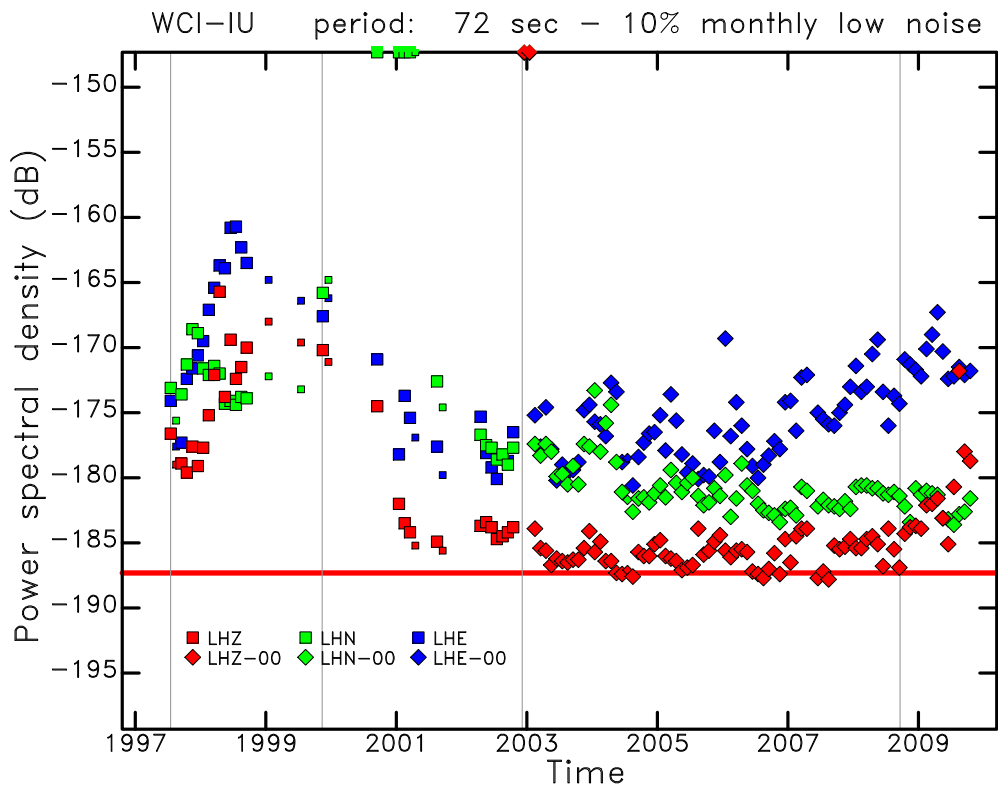
Figure 3: Diagram shows the monthly PSD of ground acceleration at 72-s period for all long-period (LH) channels at WCI for the period 1997–2009. Smaller symbols are used for months with fewer available hourly measurements. Each component is represented by a distinct symbol and color. The red horizontal line indicates the level of Peterson's (1993) Low Noise Model (LNM) at 72 s. The thin vertical lines show the times of epoch boundaries in the station metadata. Note the dramatic increase in noise levels during the year following installation (1997–1998), and since 2007, particularly on the E–W component.

Figure 4: Diagram shows the monthly PSD of ground acceleration at 193-s period for all long-period (LH) channels at WCI for the period 1988–2009. Smaller symbols are used for months with fewer available hourly measurements. Each component is represented by a distinct symbol and color. The red horizontal line indicates the level of Peterson's (1993) Low Noise Model (LNM) at 193 s. The thin vertical lines show the times of epoch boundaries in the station metadata. Note the large temporal variations and the unrealistically low vertical noise levels in 2003–2008. The vertical component shows increasing noise levels beginning in 2008.
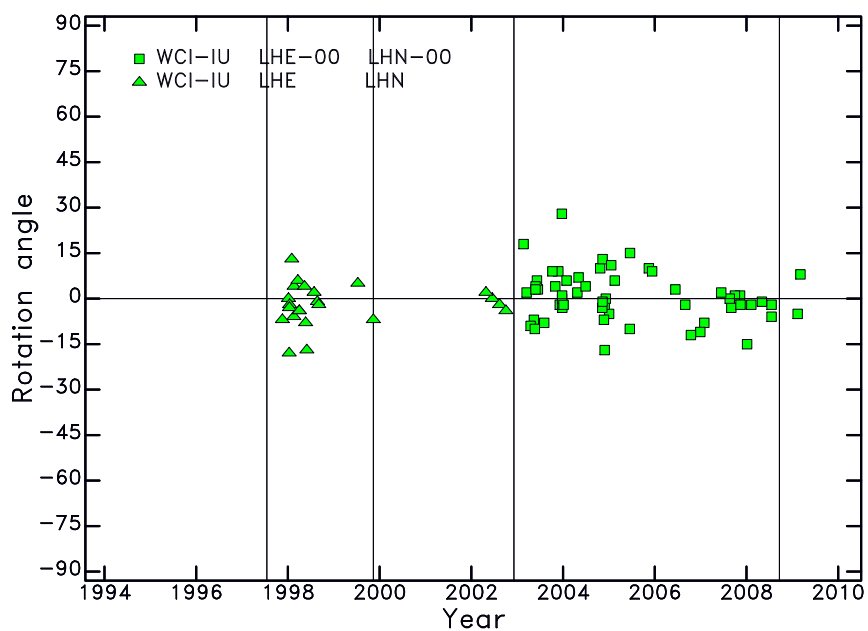
9

Figure 5: Individual measurements of polarization angle as a function of time. All measurements for the period of operation are shown. Symbols represent measurements obtained in the surface-wave band of the CMT analysis. The thin vertical lines show the times of epoch boundaries in the station metadata.
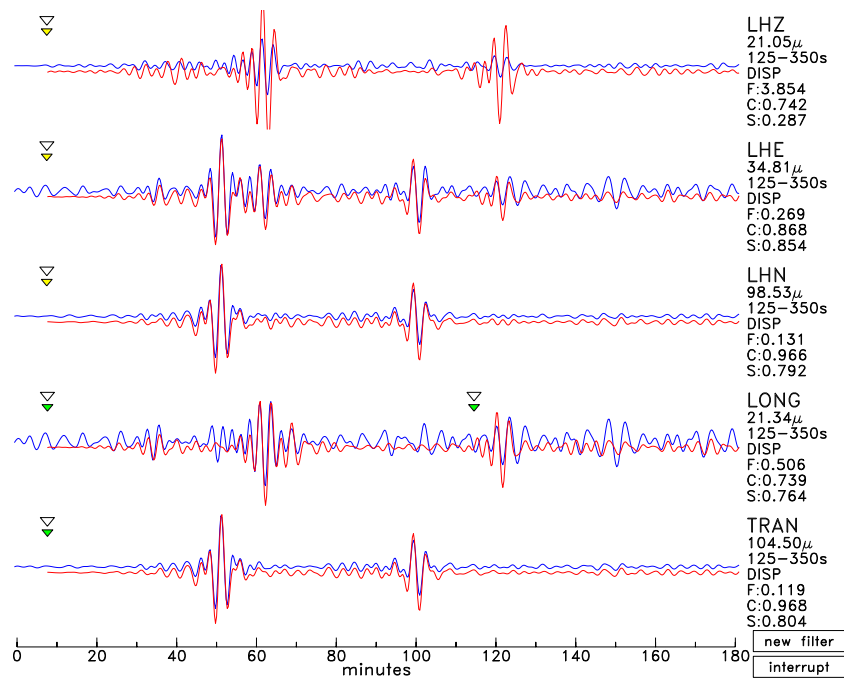
Figure 6: Comparison of observed (blue traces) and synthetic (red traces) mantle-wave seismograms recorded on the STS-1 sensor for an earthquake on December 22, 1997, a few months after instrument installation. The channel name, maximum displacement, and values for the three parameters residual misfit (F), correlation (C) and scaling factor (S) are given to the right of each waveform. The vertical component is poorly fit, with the observed seismogram having an amplitude that is approximately 1/4 of that predicted. The horizontal components are adequately fit.
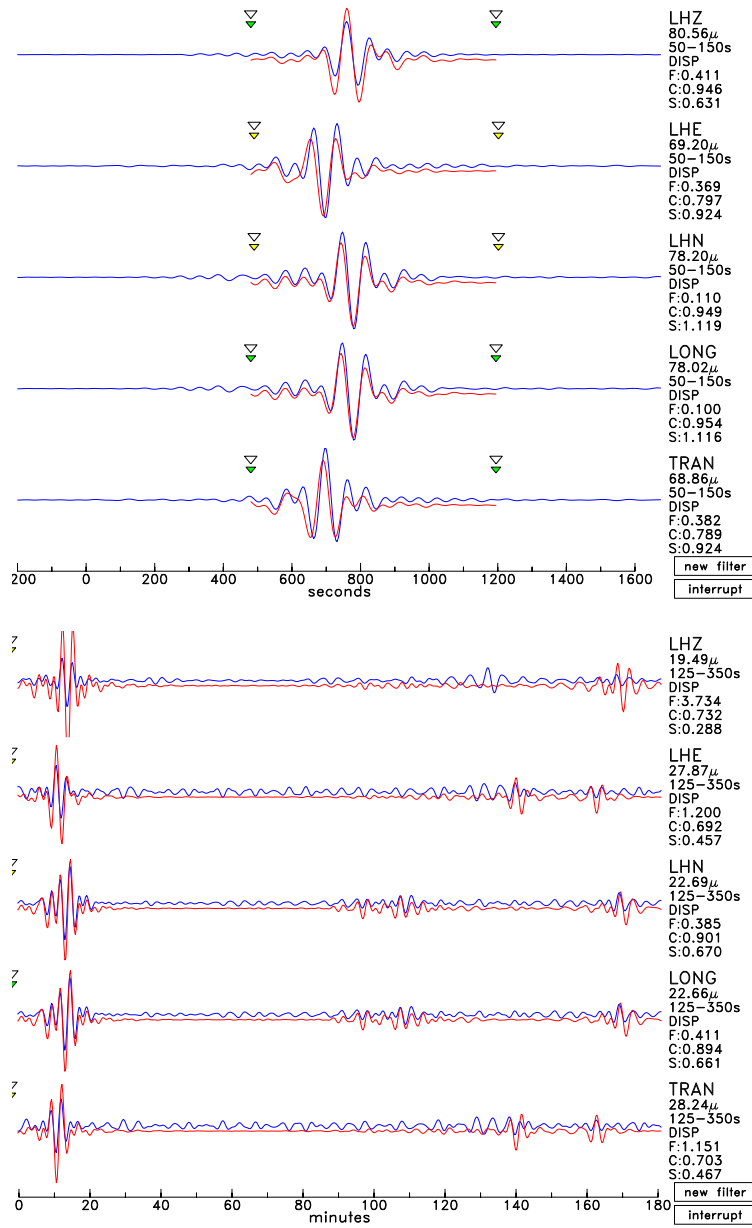
11

Figure 7: (Top) Observed and synthetic surface-wave seismograms for an earthquake on August 23, 1998, approximately one year after station installation. All components are reasonably well fit in this period band, although the observed vertical seismogram is small. (Bottom) Mantle-wave seismograms for the same earthquake. The observed vertical and E–W seismograms are too small, with scaling factors less than 0.5. The N–S seismogram has a scaling factor of 0.67. All components show evidence of gain loss at long periods, with related phase errors.
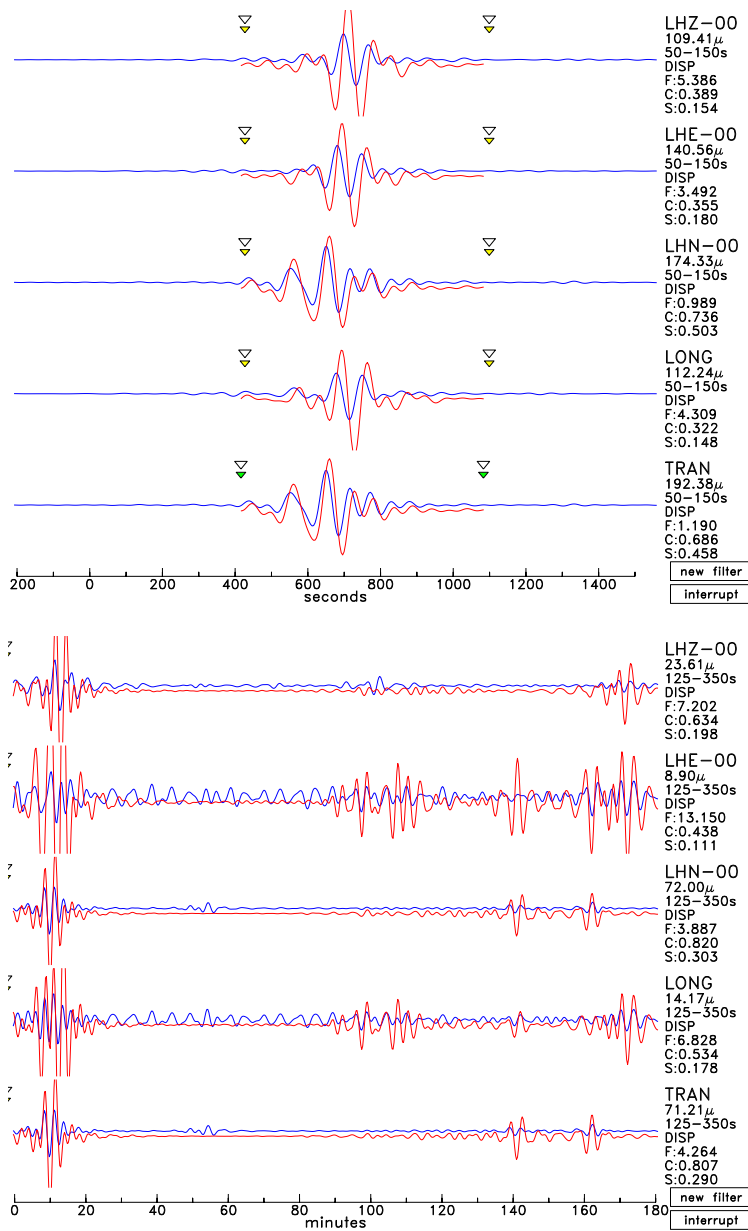
Figure 8: (Top) Observed and synthetic surface-wave seismograms for an earthquake on August 3, 2009. The fit is poor on all components, even in this shorter-period band. (Bottom) Mantle-wave seismograms for the same earthquake. Very large differences between observed and synthetic waveforms are observed. The long-period response of the seismometers is grossly incorrect.